Control Design of Passive Grid-Forming Inverters in Port-Hamiltonian Framework

Le Kong , *Member, IEEE*, Yaosuo Xue , *Senior Member, IEEE*, Liang Qiao , *Graduate Student Member, IEEE*, and Fei Wang , *Fellow, IEEE*

Abstract—This article presents a modified dispatchable virtual oscillator control approach for achieving the passivity of grid-forming inverters (GFMs), without assuming constant voltage and constant frequency. The proposed control framework utilizes the port-Hamiltonian (PH)–based structure that mimics the behaviors of coupled harmonic oscillators, along with an energy "*pumping-or-damping*" block and the control by interconnection technique, to render the inverter passive. Once passivity is achieved, the transient stability of the system will be guaranteed. The proposed control framework is composed of three loops: an outer power dispatching loop that generates the voltage and frequency references, a virtual oscillator loop that emulates the spontaneous synchronization of oscillators, and an inductor current loop that maintains lossless interconnection in PH systems. The study shows that the proposed control approach ensures the passivity of GFMs, facilitating the transient stability design of multi-inverter systems, as interconnections of passive systems remain passive and stable.

Index Terms—Grid-forming inverters, passivity, port-Hamiltonian (PH) systems, virtual oscillator control.

I. INTRODUCTION

WITH the increase of power electronics interface renewable energy and energy storage sources, power systems face new stability issues caused by the wide control bandwidth of power electronic devices and low system inertia [1], [2]. To ensure system stability and reliability, proper control strategies must be designed for power electronic inverters. Researchers have highlighted the necessity of grid-forming inverters (GFMs), which directly control the system voltage, for stable and reliable operations of future power electronics-dominated power systems [3], [4]. Therefore, this article will concentrate on investigating grid-forming control strategies.

Although GFMs can help maintain the stability of power electronics-based power system, designing proper control strategies for GFMs to ensure stability under various operating conditions remain challenging, especially when multiple inverters are operating together, or when system information is not readily available. For instance, the conventional grid-forming control approaches might have system transient stability issues due to the virtual inertia term in the controller (e.g., low-pass filters (LPFs) in droop control), or the sharp control voltage drop in the event of fault conditions (e.g., slow oscillation convergence speed of dispatchable virtual oscillator control) [5], [6].

In addressing the stability issues of GFMs under various grid conditions, the passivity-based port-Hamiltonian (PH) system theory presents a promising solution with several advantages [7], [8], [9]. First, the passive components within power transmission and distribution networks are naturally passive in terms of terminal voltage and current (i.e., impedance). Second, the passivity properties are obtained at the input or output ports of each subsystem, enabling a feasible and straightforward stability design for the interconnection of multiple inverters. In other words, if all the inverters are ensured passive, the stability of the entire system can be guaranteed through passive interconnections.

So far, various control approaches have been proposed in the literature to achieve a passivity-based design for GFMs, as summarized in Table I. These approaches are characterized by three aspects: system analysis approaches; linearity; and stability issues. While most research has focused on mitigating system small-signal high-frequency harmonic issues through linear control methods, few have focused on enhancing system transient stability. To be specific, the previous approaches have developed linear control approaches to passivate the output impedance of the inverters, as demonstrated in [10], [11], and [12], but these methods only aimed to solve small-signal high-frequency harmonic instability problems. A passivity-based dual-loop vector voltage and current control have been developed in [13], which was to mitigate the adverse effects of control time delay and to passivate the inverter impedance at a high-frequency range while disregarding the dynamics of the outer power loop. The research work in [14] focused on enhancing the small-signal phase synchronization stability of the system by passivating the

TABLE I
REVIEW OF EXISTING PASSIVITY-BASED CONTROL DESIGN FOR GFMS

Analysis Approaches	Linearity	Solved Stability Issues	Refs
Impedance-based passivity	Linear	High-frequency harmonic instabilities	[10-13]
Transfer function-based passivity	Linear	Low-frequency synchronization stability	[14]
Impedance-based passivity	Linear	Low-frequency synchronization stability	[15]
PH-based passivity	Nonlinear	Instabilities induced by inner loops	[16]
Output-differential passivity	Nonlinear	Transient stability	[17]
PH-based passivity	Nonlinear	Transient stability	[18]

transfer function of the inverter from its fundamental frequency to its active power. In [15], the low-frequency passivity behaviors of GFMs are investigated and it was observed that GFMs exhibit inherent nonpassivity in terms of small-signal output impedance due to the integral relationship between frequency and angle in the output power loop. Also, it reveals that the virtual reactance method proves effective in enhancing the inverter passivity index. In [16], a control approach for GFMs was developed using the PH-based passivity theory, which considered the impact of nonlinear loads. However, this was limited to the fast dynamics of the inner current loops assuming that the system was always well synchronized with the grid (i.e., constant voltage and constant frequency). A distributed stability criterion was proposed in [17] based on the output-differential passivity in terms of bus voltage and bus power, but determining the passivity of GFMs with different types of controls was challenging and the power flow data was required for the evaluation of the passivity index of the entire system. In [18], a PH-based passive virtual synchronous machine control strategy was introduced, which did not require the assumption of constant voltage and constant frequency. However, the three-channel structure of the control approach was complicated, and the relationships between passivity and system stability were still uncertain. Thus, it is desirable to develop a simpler control structure that preserves inverter passivity while retaining physical significance using conventional control variables such as active power and reactive power. Also, the relationships between inverter passivity and system stability are expected to be revealed.

Accordingly, this article proposes a PH-based two-channel control structure using active power, reactive power, and voltage as the control variables for the passivity design of GFMs. The main contributions could be summarized as follows.

1) Devising a simple control structure that is compatible with other grid-forming control strategies, such as droop control, or virtual oscillator control.
2) Rendering the GFMs passive without the assumption of constant voltage and constant frequency, thus, improving system transient stability under various transient scenarios.
3) Exploring the relationships between inverter passivity and system transient stability.

The rest of the article is organized as follows. Section II provides a brief review of the passivity-based PH system theory and typical grid-forming control laws. In Section III, the proposed control structure is given with the proof of passivity of GFMs in the closed loop with discussions on the controller implementation issues. In Section IV, the proposed control approach is compared with the dVOC method in terms of passivity and transient stability. Section V presents simulation and experimental case studies to validate the effectiveness of the proposed strategy in maintaining the stability of multi-inverter systems. Finally, Section VI concludes this article.

II. PRELIMINARIES

A. Principles of Port-Hamiltonian Control Theory

Consider a general input–output nonlinear dynamical system $S : u \rightarrow y$ described as described by

$$\begin{cases} \dot{x} = f(x, u) \\ y = h(x, u) \end{cases} \tag{1}$$

where $x \in \mathbb{R}^n$, $u \in \mathbb{R}^m$, and $y \in \mathbb{R}^m$. The system S is passive if there exists a storage function $H(x)$ bounded from below such that $H(x(t_2)) - H(x(t_1)) \leq \int_{t_1}^{t_2} u^T(t)y(t)dt$ and $t_1 \leq t_2$. If H is differentiable, then $\dot{H} \leq u^T y$. This property characterizes the energy dissipation behavior of the system S. It implies that the system S cannot generate energy and that any energy stored in the system must be dissipated over time.

To construct the storage function H for a nonlinear system, it is often helpful to reformulate the system's ordinary differential equations (ODEs) into a known framework [19], such as the Euler–Lagrange framework, the PH framework, the Brayton–Moser framework, etc. In this article, the PH framework is selected since its ODEs are first-order equations that are easier to solve than some high-order expressions [20], [21].

A PH system can be written as

$$\sum : \begin{cases} \dot{x} = (\mathcal{J}(x) - \mathcal{R}(x)) \frac{\partial H}{\partial x}(x) + g(x) u \\ y = g^T(x) \frac{\partial H}{\partial x}(x) \end{cases} \tag{2}$$

where the interconnection matrix $\mathcal{J}$ is skew-symmetric (i.e., $\mathcal{J}(x) = -\mathcal{J}^T(x)$), and $\frac{\partial H}{\partial x}(x)$ is the column vector of partial derivatives [20]. Note that with $\mathcal{R}(x) = \mathcal{R}^T(x) \geq 0$ specifying the energy dissipation, the system is passive with storage function H satisfying $\dot{H} = u^T y - \frac{\partial H^T}{\partial x} \mathcal{R}(x) \frac{\partial H}{\partial x} \leq u^T y$.

Furthermore, the feedback interconnection of two passive systems (i.e., $\dot{H}_1 \leq u_1^T y_1$, $\dot{H}_2 \leq u_2^T y_2$, $u_1 = -y_2 + v_1$, $u_2 = -y_1 + v_2$) leads to a passive interconnected system since $\dot{H}_1 +$
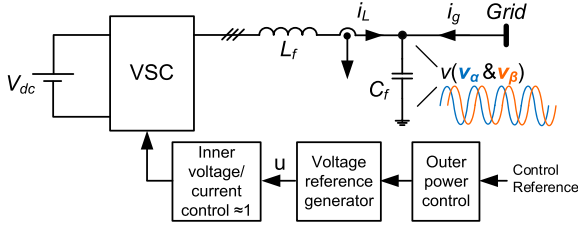
Fig. 1   Grid-connected grid-forming inverter.

$\dot{H}_2 \leq v_1^T y_1 + v_2^T y_2$, where v_1 and v_2 are the external inputs for these two passive systems separately.

B. Typical Grid-Forming Control Laws

The single-line diagram of a general three-phase GFM connecting to the grid is illustrated in Fig. 1. The inverter has an LC output filter with inductor current denoted as i_L and capacitor voltage denoted as v. The control input for the GFM is u and the external disturbance is grid current i_g. The system will be conducted in the stationary $\alpha\beta$ reference frame, which is transformed from the abc reference frame using the Clarke transformation.

Given the decoupled timescale between the inner voltage/current loop and the outer power loop, the dynamics of the inner loop can be disregarded and treated as a unity gain component because the focus of this article is on system transient stability. Additionally, the switching effect of the power switches will be neglected based on the averaging theory.

For the outer power loop, various control structures have been developed so far [22]. Among the typical control structures are: power-synchronization control (PSC) [23], [24], basic droop control [25], [26], [27], droop control with LPFs [28], [29], and dispatchable virtual oscillator control [30], [31], [32], [33], [34]. The characteristics of each control structure can be thoroughly investigated by employing the control law equations in polar coordinates. The control laws of PSC and basic droop control can be both described as

$$\begin{cases} \dot{\theta} = \omega_0 + m_P \left(P_0 - P \right) \\ u = u_o + n_Q \left(Q_0 - Q \right) \end{cases} \tag{3}$$

where m_P and n_Q are the control gains, and P_0 and Q_0 are the active power and reactive power of the inverter, respectively. The control laws of droop control with LPFs can be represented by

$$\begin{cases} \dot{\theta} = \omega_0 + m_P \frac{\omega_P}{s+\omega_P} \left(P_0 - P \right) \\ u = u_o + n_Q \frac{\omega_Q}{s+\omega_Q} \left(Q_0 - Q \right) \end{cases} \tag{4}$$

where ω_P and ω_Q are the cutoff frequencies of the active and reactive power loops. The control laws of dispatchable virtual oscillator control in [33] can be represented by

$$\begin{cases} \dot{\theta} = \omega_0 + \frac{m_P}{u^2} \left(P_0 - P \right) \\ \dot{u} = \frac{k_u}{u_{\text{ref}}^2} \left(u_{\text{ref}}^2 - u^2 \right) u + \frac{n_Q}{u} \left(Q_0 - Q \right) \end{cases} \tag{5}$$

where k_u is the control gain of the internal voltage oscillator. Another type of dVOC control in [32] and [34] can be described by

$$\begin{cases} \dot{\theta} = \omega_0 + m_P \left(\frac{P_{\text{ref}}}{u_{ref}^2} - \frac{P(u)\sin\delta}{u^2} \right) \\ \dot{u} = \frac{k_u}{u_{\text{ref}}^2} \left(u_{\text{ref}}^2 - u^2 \right) u + n_Q \left(\frac{Q_{\text{ref}}}{u_{\text{ref}}^2} - \frac{Q(u,\delta)}{u^2} \right) u. \end{cases} \tag{6}$$

Among the control methods mentioned, the droop control with LPFs described in (4) may lose synchronism after disturbances due to the virtual inertia terms introduced by LPFs [5], [6]. However, if the cutoff frequencies of the LPFs are sufficiently high, (4) could be considered similar to the approach in (3). The PSC or basic droop control can ensure system transient stability as long as equilibrium points exist following significant disturbances, assuming a constant voltage. However, the dynamics of *reactive power-voltage* interactions can potentially jeopardize system stability. The dVOC approach in [32] and [34] has also been shown to have better transient stability than droop control with LPFs due to its heavily damped *active power-frequency* control performance [5], [35]. However, it may also become unstable due to the significant voltage drop in the *reactive power-voltage* loop during certain transient events. By examining equations from (3) to (6), it can be observed that the dVOC approach resembles a typical droop controller around the nominal operating point $u \approx u_{\text{ref}} = 1$ [34], [36], [37], [38]. Hence, the equation in (6) can be regarded as encompassing all the dynamics described in (3)–(5).

Therefore, the objective of this article is to propose a control methodology that achieves passivation for the control law described in (6), by utilizing the principles of PH control theory. Note that inductive transmission lines are assumed for the control laws discussed above, as well as for the subsequent analysis conducted throughout this article. However, with suitable decoupling assumptions, the approach proposed in this manuscript can be effectively extended to resistive grids. Like other dVOC approaches [32], [38], the extension can be achieved by mainly considering the dynamics of P - u and Q - θ within resistive grids, applying the same theoretical framework used for examining dynamics of P - θ and Q - u within inductive grids. It is also worth mentioning that the specific type of the virtual synchronous generator control [39], [40] is not addressed in this article and its passivity-based design can be found in [18] as already been discussed in Section I.

III. Proposed PH-Based Control Framework and Passivity Analysis of GFMs

A. Modeling of Open-Loop GFM and Passivity Analysis

Assuming a constant control input u, the inverter will operate in open-loop mode. The system PH-based model can then be represented by

$$\sum_P : \begin{cases} \dot{x}_P = \left(\mathcal{J}_P - \mathcal{R}_P \right) \nabla H_P \left(x \right) + Gu + K\xi \\ y_{P1} = G^T \nabla H_P \left(x \right) \\ y_{P2} = K^T \nabla H_P \left(x \right) \end{cases} \tag{7}$$

with the inductor flux and capacitor charge as the state variables $x_P = [\varphi_{L\alpha} \quad \varphi_{L\beta} \quad q_\alpha \quad q_\beta]^T$ and the Hamiltonian function as given by

$$H_P(x) = \frac{1}{2}L_f i_{L\alpha}^2 + \frac{1}{2}L_f i_{L\beta}^2 + \frac{1}{2}C_f v_\alpha^2 + \frac{1}{2}C_f v_\beta^2 \quad (8)$$

where $\mathcal{J}_P = \begin{bmatrix} 0 & 0 & -1 & 0 \\ 0 & 0 & 0 & -1 \\ 1 & 0 & 0 & 0 \\ 0 & 1 & 0 & 0 \end{bmatrix}$, $\mathcal{R}_P = \begin{bmatrix} R_f & 0 & 0 & 0 \\ 0 & R_f & 0 & 0 \\ 0 & 0 & 0 & 0 \\ 0 & 0 & 0 & 0 \end{bmatrix}$, $G = \begin{bmatrix} 1 & 0 \\ 0 & 1 \\ 0 & 0 \\ 0 & 0 \end{bmatrix}$, $K = \begin{bmatrix} 0 & 0 \\ 0 & 0 \\ 1 & 0 \\ 0 & 1 \end{bmatrix}$, $u = \begin{bmatrix} u_\alpha \\ u_\beta \end{bmatrix}$, and $\xi = \begin{bmatrix} i_{g\alpha} \\ i_{g\beta} \end{bmatrix}$.

It is obvious that the PH system in (7) is passive with $H_P(x) \geq 0$ in terms of system inputs ($[u^T \quad \xi^T]^T$) and system outputs ($[y_{P1}^T \quad y_{P2}^T]^T$).

B. Proposed Control Block With Control by Interconnection Technique

The analysis above shows that an open-loop inverter is passive, as the damping matrix $\mathcal{R}_P$ is nonnegative (i.e., $R_f \geq 0$) and interconnection matrix $\mathcal{J}_P$ is skew-symmetric. To make the closed-loop inverter passive, the control by interconnection (CbI) technique [41] can be utilized. In CbI, the control block is treated as another PH system with its own state variables and Hamiltonian function. The controller is then connected with the inverter plant in a lossless manner. This means that the input and output pairs of both the inverter and the controller are power preserving, as "*lossless interconnection*" is a mathematical concept. For example, the feedback interconnection of two passive systems as introduced in Section II-A can be considered as a lossless interconnection. The energy function of the closed-loop system can then be considered as the sum of the Hamiltonian functions of the open-loop system and the controller, thus ensuring the closed-loop system is passive.

When designing the control for GFMs, the open-loop PH model takes the control voltage u as the input and the inductor current i_L as the output. Hence, to preserve power in the interconnection of the controller and the inverter plant, the simplest way is to choose the inductor current i_L as the input and the control voltage u as the output for the controller. By doing so, the product $u \times i_L$ of the inverter plant is equivalent to $i_L \times u$ of the controller, without requiring any additional external inputs.

Accordingly, a control framework can be proposed, as shown in Fig. 2, which is developed based on the concept of dVOC, but with enhanced transient stability using the passivity-based design approach.

The proposed control approach comprises three loops: the outer power loop, the virtual oscillator loop, and the inductor current loop.

The outer power loop consists of two channels: the active power loop, which generates the frequency reference with a constant gain ξ_3, and the reactive power channel, which adjusts the oscillation magnitude of the virtual oscillator with a sign-indefinite gain $\pm|\xi_2|$. It is important to note that this
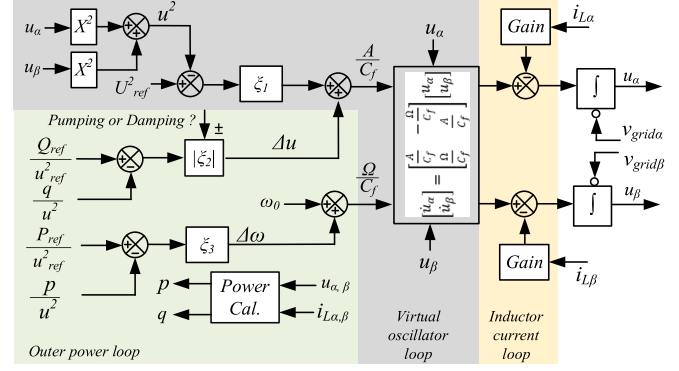

Fig. 2.   Proposed control scheme.

sign-indefinite gain $\pm|\xi_2|$ in the outer reactive power loop creates a "*pumping-or-damping*" motion, achieving a nonnegative damping matrix, and allowing for a passive design of GFMs.

The virtual oscillator loop is responsible for mimicking the dynamics of coupled harmonic oscillators to achieve spontaneous synchronization of multiple inverters, similar to other virtual oscillator-based control [32], [34].

The inductor current loop maintains the lossless interconnection between the controller block and the inverter plant block, ensuring that $u \times i_L = i_L \times u$. The control gain of the current loop is extremely small in the proposed control structure, as its only purpose is to maintain lossless interconnection mathematically, while not affecting the control performance of the outer power loop and the virtual oscillator loop. Note that the inductor current loop here should not be confused with the conventional fast inner current loop as described in Fig. 1 since its purpose is solely for lossless interconnection in the PH system in a mathematical sense.

By adding the energy functions of the inverter plant and the controller, the closed-loop energy function can be simply obtained. Further details will be explained in Section III-C.

The dynamic equations of the proposed control can be represented by

$$\sum\nolimits_C : \dot{x}_C = \left(\begin{bmatrix} -\varepsilon^2/\Phi & 0 & 0 & -\Omega \\ 0 & -\varepsilon^2/\Phi & \Omega & 0 \end{bmatrix} \right.$$
$$\left. - \begin{bmatrix} 0 & 0 & -A & 0 \\ 0 & 0 & 0 & -A \end{bmatrix} \right) \begin{bmatrix} \dot{i}_{L\alpha} \\ \dot{i}_{L\beta} \\ u_\alpha \\ u_\beta \end{bmatrix} \quad (9)$$

where the control state variables are denoted as $x_C = [C_f u_\alpha \quad C_f u_\beta]^T$. The voltage-amplitude-related term of the virtual oscillator A is defined by

$$A = C_f \xi_1 \left(u_{\text{ref}}^2 - u^2 \right) + C_f \text{sgn}(\xi_2) |\xi_2| \left(\frac{Q_{\text{ref}}}{u_{\text{ref}}^2} - \frac{Q}{u^2} \right) \quad (10)$$

and the frequency-related term of the virtual oscillator Ω is defined by

$$\Omega = \omega_o C_f + \xi_3 C_f \left(\frac{P_{\text{ref}}}{u_{\text{ref}}^2} - \frac{P}{u^2} \right). \quad (11)$$
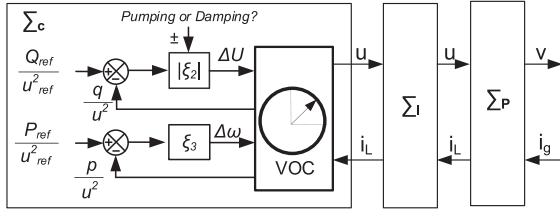
Fig. 3.   Closed-loop GFMs in the PH framework.

The Hamiltonian function $H_C(x)$ is defined by

$$H_C(x) = \frac{1}{2} \frac{\Phi^2}{\varepsilon^2} \tag{12}$$

where ε is a small constant and Φ is defined by

$$\Phi = \frac{1}{2}C_f u_\alpha^2 + \frac{1}{2}C_f u_\beta^2 - \frac{1}{2}C_f u_{\text{ref}}^2 = \frac{1}{2}C_f\left(u^2 - u_{\text{ref}}^2\right). \tag{13}$$

The reason that ε is designed to be small is to counteract the small value of Φ (i.e., when u close to u_{ref}), which can be described by $\lim\limits_{\varepsilon \to 0, \Phi \to 0} -\varepsilon^2/\Phi = -\varepsilon$. This property enables the practical implementation of the current loop by simply multiplying a small gain.

C. Modeling of Closed-Loop GFMs With the Proposed Control Block and Passivity Analysis

With the proposed control strategy, the closed-loop system can then be represented in the PH framework as shown in Fig. 3. It consists of a control block Σ_C, an interconnection block Σ_I, and a plant block Σ_P.

The closed-loop system can also be modeled by

$$\sum : \begin{cases} \begin{bmatrix} \dot{x}_P \\ \dot{x}_c \end{bmatrix} = (\mathcal{J} - \mathcal{R})\nabla H(x) + L\xi \\ y = L^T \nabla H(x) \end{cases} \tag{14}$$

where $\mathcal{J} = \begin{bmatrix} 0 & 0 & -1 & 0 & \varepsilon^2/\Phi & 0 \\ 0 & 0 & 0 & -1 & 0 & \varepsilon^2/\Phi \\ 1 & 0 & 0 & 0 & 0 & 0 \\ 0 & 1 & 0 & 0 & 0 & 0 \\ -\varepsilon^2/\Phi & 0 & 0 & 0 & 0 & -\Omega\varepsilon^2/\Phi \\ 0 & -\varepsilon^2/\Phi & 0 & 0 & \Omega\varepsilon^2/\Phi & 0 \end{bmatrix}$, $\mathcal{R} =$

$\begin{bmatrix} R_f & 0 & 0 & 0 & 0 & 0 \\ 0 & R_f & 0 & 0 & 0 & 0 \\ 0 & 0 & 0 & 0 & 0 & 0 \\ 0 & 0 & 0 & 0 & 0 & 0 \\ 0 & 0 & 0 & 0 & -A\varepsilon^2/\Phi & 0 \\ 0 & 0 & 0 & 0 & 0 & -A\varepsilon^2/\Phi \end{bmatrix}$, and $L = \begin{bmatrix} 0 & 0 \\ 0 & 0 \\ 1 & 0 \\ 0 & 1 \\ 0 & 0 \\ 0 & 0 \end{bmatrix}$.

The closed-loop energy function H is defined by

$$H = H_P + H_c. \tag{15}$$

As can be seen, the interconnection matrix is skew-symmetric (i.e., $\mathcal{J} = -\mathcal{J}^T$), due to the lossless interconnection through the inductor current loop. With a nonnegative damping matrix

$\mathcal{R}$ (i.e., $\mathcal{R} \geq 0$), the derivative of H can be represented by

$$\dot{H} = \xi^T y - \frac{\partial H^T}{\partial x}\mathcal{R}\frac{\partial H}{\partial x} \leq \xi^T y \tag{16}$$

which indicates that the closed-loop system described by (14) is passive concerning the inputs $\xi = \begin{bmatrix} i_{g\alpha} & i_{g\beta} \end{bmatrix}^T$ and the outputs $y = \begin{bmatrix} v_\alpha & v_\beta \end{bmatrix}^T$. It should be noted that the passivity design discussed in this article addresses the transient stability of the inverter in a system. The focus is on studying dynamic interactions between the outer power loop of the inverter and the grid under various grid conditions.

To ensure that the damping matrix $\mathcal{R} \geq 0$, either $-A\varepsilon^2/\Phi$ or $-A/\Phi$ must be nonnegative, which implies that the value of A needs to be adjusted based on the changes of Φ. By defining the passivity-related index $K_P = -A/\Phi$ and based on (10) and (13), K_P can be represented by

$$K_P = 2\xi_1 - 2\text{sgn}(\xi_2)|\xi_2|\left(\frac{Q_{\text{ref}}}{u_{\text{ref}}^2} - \frac{Q}{u^2}\right)/\left(u^2 - u_{\text{ref}}^2\right). \tag{17}$$

It can be observed that the first term $2\xi_1$ will always be nonnegative if ξ_1 is designed to be positive. Additionally, $\text{sgn}(\xi_2)|\xi_2|$ should be sign-indefinite and determined by

$$\text{sgn}(\xi_2) = -\text{sgn}\left(\frac{\left(\frac{Q_{\text{ref}}}{u_{\text{ref}}^2} - \frac{Q}{u^2}\right)}{(u^2 - u_{\text{ref}}^2)}\right). \tag{18}$$

Specifically, if $\Phi > 0$, $\text{sgn}(\xi_2)|\xi_2|$ should be adjusted to damp the energy; if $\Phi < 0$, $\text{sgn}(\xi_2)|\xi_2|$ should be tuned to pump the energy. Thus, a "*pumping-or-damping*" motion is adopted in the reactive power loop to maintain the nonnegativity of the damping matrix $\mathcal{R}$. Although this is a conservative design, it ensures the passivity of the inverter and, consequently, the transient stability of the system. Additionally, (17) and (18) become undefined when $u = u_{\text{ref}}$ as they involve division by zero. Nevertheless, this uncertainty does not affect the normal operation of the controller, as will be further discussed in Sections III-D and IV-B, respectively.

D. Discussions of Controller Implementation

Based on the analysis above, the dynamics of control voltage u in $\alpha\beta$ axis can be described by

$$\begin{cases} \dot{u}_\alpha = -\frac{\varepsilon^2}{C_f\Phi}\dot{i}_{L\alpha} + \frac{A}{C_f}u_\alpha - \frac{\Omega}{C_f}u_\beta \\ \dot{u}_\beta = -\frac{\varepsilon^2}{C_f\Phi}\dot{i}_{L\beta} + \frac{A}{C_f}u_\beta + \frac{\Omega}{C_f}u_\alpha \end{cases} \tag{19}$$

where A is given in (10), Ω is defined in (11), and Φ is defined in (13). As can be seen, the inductor current gain in the proposed control structure is $\frac{\varepsilon^2}{C_f\Phi}$, where ε is an extremely small value. This small gain ε can be selected to match the least significant bit value of the digital signal processor employed in the system.

For the selection of control parameters ξ_1 and ξ_2 in A and control parameter ξ_3 in Ω of the proposed approach, similar procedures can be adopted as those for dVOC in [30] and [33] since they share a similar control structure, except for the "*pumping-or-damping*" block and the inductor current loop for lossless interconnection. The parameter ξ_1 is related with the
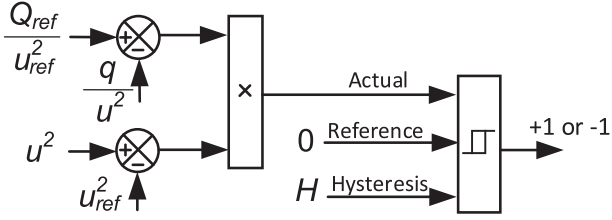
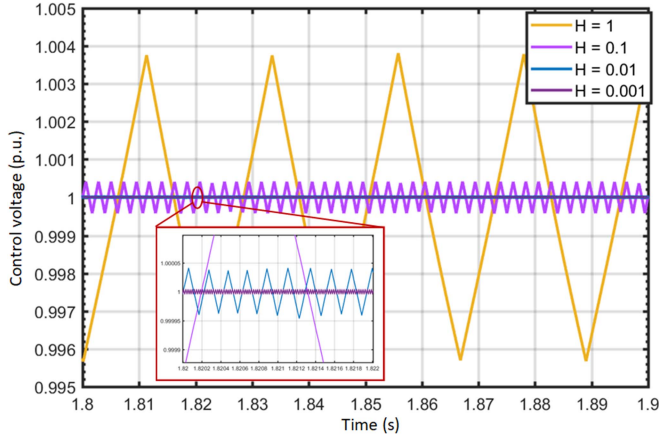Fig. 4. Control diagram of the "*pumping or damping*" block.

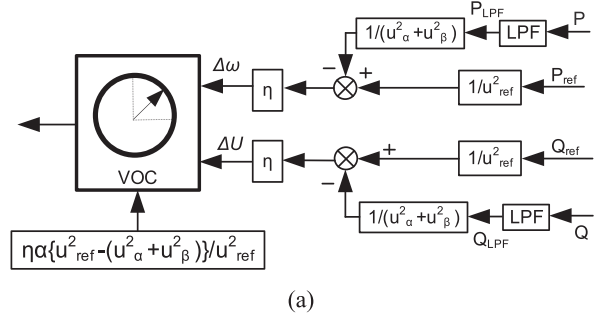Fig. 5. Magnitude of control voltage with different hysteresis values.

(a)

(b)

Fig. 6. Control diagrams. (a) dVOC approach in [32] and [34]. (b) Simplified proposed approach.

convergence speed of the virtual oscillator loop when unloaded. For example, if the time taken for the voltage to rise from $0.1u_{\text{ref}}$ to $0.9u_{\text{ref}}$ is defined as t_{rise}, then ξ_1 can be calculated by

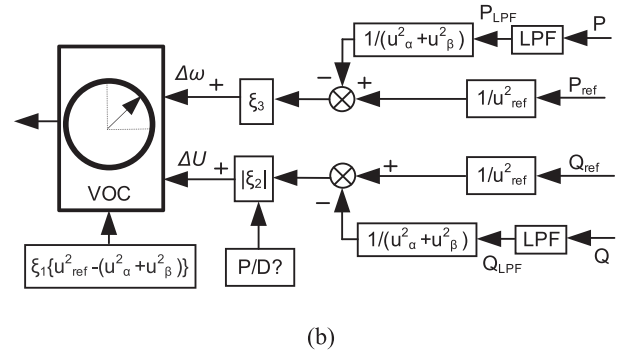$$\xi_1 = \frac{3}{t_{\text{rise}} \times u_{\text{ref}}^2}. \tag{20}$$

The selection of ξ_2 and ξ_3 can equivalently follow the design of basic droop control in (3). The main difference is that the proposed approach has sign-indefinite ξ_2 due to the "*pumping or damping*" motion.

To implement the sign-indefinite "*pumping or damping*" action as described in (18), a hysteresis block is used for the transition between $+\xi_2$ and $-\xi_2$, similar to other bang-bang control schemes. Fig. 4 illustrates this implementation, where H is the preset hysteresis value. Since the actual signal is compared with the reference value, which is 0, the hysteresis value could be selected to be close to 0.

The impact of different hysteresis values (e.g., 0.001, 0.01, 0.1, and 1) on the magnitude of the control voltage is shown in Fig. 5. As the hysteresis band increases, the voltage magnitude variation also increases. In the given example, the largest voltage variation happens when the hysteresis value is set as 1, but it is still small enough to be ignored compared with the system reference control voltage, which is approximately $\pm 0.4\%$ of the system control voltage. From Fig. 5, it can also be observed that, in the vicinity of u_{ref} (i.e., $u \to u_{\text{ref}}$), the behavior of u is undefined. It may either increase or decrease, rather than remain fixed, which is affected by $\text{sgn}(\xi_2)$.

Additionally, it is worth noting that in the practical implementation of (18), a multiplier is utilized instead of a divider for $\frac{Q_{\text{ref}}}{u_{\text{ref}}^2} - \frac{Q}{u^2}$ and $u^2 - u_{\text{ref}}^2$. This is done for two reasons. First, the choice between multiplication and division does not impact the sign determination. Second, multiplication is generally faster than division in digital controllers.

IV. PASSIVITY AND TRANSIENT STABILITY OF PROPOSED APPROACH COMPARING WITH THE dVOC APPROACH

A. Passivity Analysis of the dVOC Approach

As reviewed in Section II-B, the dVOC approach shows advantages in transient stability compared to other existing approaches. The proposed method is developed upon the dVOC approach. Therefore, in this section, comparisons will be conducted between the proposed method and the dVOC approach. The control law of dVOC in polar coordinates is shown in Fig. 6(a). As discussed in [32] and [34], it could be designed to be almost globally asymptotically stable for a prespecified ac power-flow solution at the system's fundamental frequency by selecting proper control parameters with system information. By comparing with the simplified control diagrams of the proposed method in Fig. 6(b) with only the outer power loops, it can be observed that the main difference between the proposed method and dVOC is the presence of the "*pumping-or-damping*" block in reactive power loop in the proposed method. It should also be noted that in real implementation, LPFs are generally added to filter out the measurement noise.

To compare the performance of the proposed method with the dVOC approach, the dVOC approach can also be rearranged in
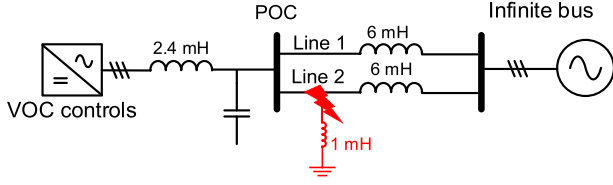
Fig. 7.   Diagrams of test bench with short-to-ground fault.

the PH framework which is represented by

$$
\sum\nolimits_{\text{dVOC}} : \begin{cases} \begin{bmatrix} \dot{x}_P \\ \dot{x}_c \end{bmatrix} = (\mathcal{J} - \mathcal{R}_{\text{dVOC}})\, \nabla H\left(x\right) + L\xi \\ y = L^T \nabla H\left(x\right) \end{cases} \tag{21}
$$

with assuming the same CbI-based inner current loop structure as the proposed control approach. In the dVOC approach, the damping matrix is changed to $\mathcal{R}_{\text{dVOC}}$ as given by

$$
\mathcal{R}_{\text{dVOC}} = \begin{bmatrix} R_f & 0 & 0 & 0 & 0 & 0 \\ 0 & R_f & 0 & 0 & 0 & 0 \\ 0 & 0 & 0 & 0 & 0 & 0 \\ 0 & 0 & 0 & 0 & 0 & 0 \\ 0 & 0 & 0 & 0 & -A_{\text{dVOC}}\varepsilon^2/\Phi & 0 \\ 0 & 0 & 0 & 0 & 0 & -A_{\text{dVOC}}\varepsilon^2/\Phi \end{bmatrix} \tag{22}
$$

with A_{dVOC} being defined as

$$
A_{\text{dVOC}} = C_f \frac{\eta\alpha}{u_{\text{ref}}^2}\left(u_{\text{ref}}^2 - u^2\right) + C_f\eta\left(\frac{Q_{\text{ref}}}{u_{\text{ref}}^2} - \frac{Q}{u^2}\right) \tag{23}
$$

while $\mathcal{J}$, L, and H remain the same as in (14). Similarly, to check if the damping matrix is positive or not, the passivity-related index $K_{P_{\text{dVOC}}}$ is defined by

$$
K_{P_{\text{dVOC}}} = -\frac{A_{\text{dVOC}}}{\Phi} = 2\frac{\eta\alpha}{u_{\text{ref}}^2} - 2\eta\left(\frac{Q_{\text{ref}}}{u_{\text{ref}}^2} - \frac{Q}{u^2}\right)\Big/\left(u^2 - u_{\text{ref}}^2\right). \tag{24}
$$

If $K_{P_{\text{dVOC}}}$ is positive, it means $\mathcal{R}_{\text{dVOC}}$ is positive and the control approach is passive. Vice versa, if $K_{P_{\text{dVOC}}}$ is negative, it means $\mathcal{R}_{\text{dVOC}}$ is negative, and the control approach is nonpassive.

B. Comparisons Between the Proposed Approach and the dVOC Approach: Passivity and Transient Stability

To further evaluate the passivity-related indices of the proposed method (K_P) and the dVOC approach ($K_{P_{\text{dVOC}}}$) in a transient event of a power system and their impact on system transient stability, a simplified test bench is implemented in MATLAB as shown in Fig. 7. In this test scenario, a short-to-ground fault occurs at Line 2 with 1 mH short impedance, and the fault is cleared after 250 ms by disconnecting Line 2. To ensure a fair comparison, the control parameters are selected to be equivalent, where $\frac{\eta\alpha}{u_{\text{ref}}^2} = \xi_1 = 0.001$ and $\eta = |\xi_2| = \xi_3 = 15$. For more details on the test system, refer to [35]. Two cases will be studied with different cutoff frequencies of the LPFs in the power loops. The cases presented can be viewed as the worst-case scenario, considering that the proposed approach aims to preserve the heavily damped characteristics of the active power-frequency control loop while addressing the challenges
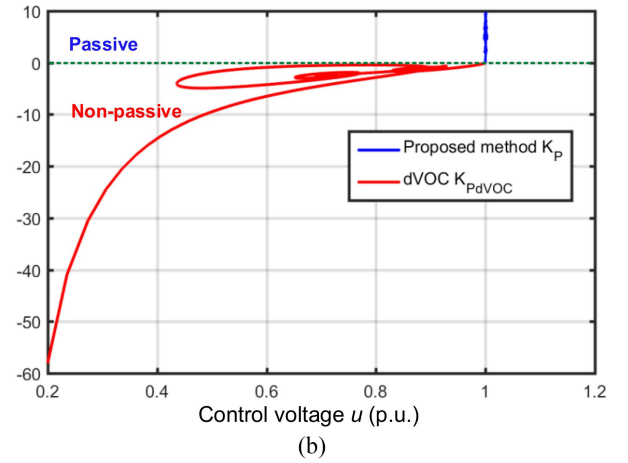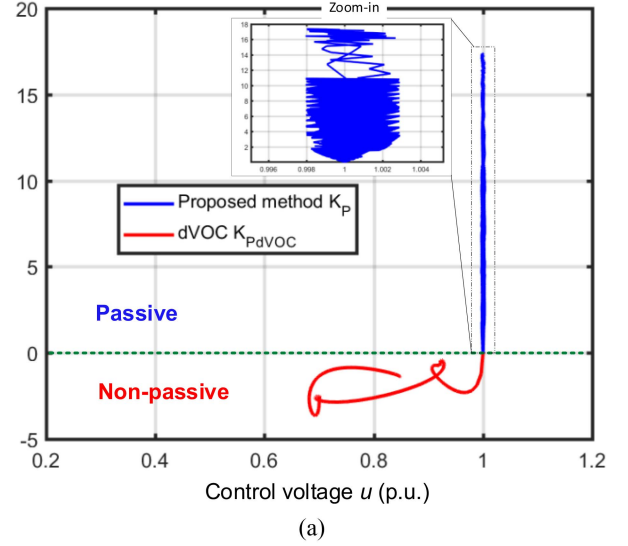

(a)

(b)

Fig. 8.   Passivity-related indices of the proposed method K_P and the dVOC approach $K_{P_{\text{dVOC}}}$ with (a) $\omega_{\text{LPF}} = 20\pi$ rad/s and (b) $\omega_{\text{LPF}} = 2\pi$ rad/s.

arising from voltage dynamics. Specifically, these cases aim to demonstrate the performance differences between the proposed approach and dVOC when a severe transient event occurs with a sharp voltage drop.

1) Passivity-Related Index: To analyze the passivity of the system during the short-to-ground transient event, the coupled dynamic equations of frequency and voltage for the proposed control are represented by

$$
\begin{cases} \dot{\delta} = \xi_3\left(\frac{P_{\text{ref}}}{u_{\text{ref}}^2} - \frac{\omega_{\text{LPF}}}{s + \omega_{\text{LPF}}}\frac{P(u)\sin\delta}{u^2}\right) \\ \dot{u} = \xi_1\left(u_{\text{ref}}^2 - u^2\right)u + \text{sgn}(\xi_2)\,|\xi_2|\left(\frac{Q_{\text{ref}}}{u_{\text{ref}}^2} - \frac{\omega_{\text{LPF}}}{s + \omega_{\text{LPF}}}\frac{Q(u,\delta)}{u^2}\right)u \end{cases} \tag{25}
$$

and the dVOC control approaches can be described by

$$
\begin{cases} \dot{\delta} = \eta\left(\frac{P_{\text{ref}}}{u_{\text{ref}}^2} - \frac{\omega_{\text{LPF}}}{s + \omega_{\text{LPF}}}\frac{P(u)\sin\delta}{u^2}\right) \\ \dot{u} = \frac{\eta\alpha}{u_{\text{ref}}^2}\left(u_{\text{ref}}^2 - u^2\right)u + \eta\left(\frac{Q_{\text{ref}}}{u_{\text{ref}}^2} - \frac{\omega_{\text{LPF}}}{s + \omega_{\text{LPF}}}\frac{Q(u,\delta)}{u^2}\right) \end{cases}. \tag{26}
$$

The passivity-related indices can then be calculated using the "ode23" solver in MATLAB. Fig. 8 presents the calculated

passivity-related indices of the proposed method and the dVOC approach during the short-to-ground fault with different cutoff frequencies of power loop LPFs. In Fig. 8(a), the cutoff frequency is 10 Hz. The results illustrate that the proposed control can ensure the control voltage u remain as the per-unit value u_{ref} before, during, and after the fault. While the behavior of $u \to u_{\text{ref}}$ leads to the indeterminacy of K_P, as described by (17), it is essential to note that K_P consistently maintains positive, meaning that the inverter is always passive throughout the operation. While $K_{P_{\text{dVOC}}}$ of the dVOC approach is negative meaning that the inverter is nonpassive, and the control voltage could drop to 0.7 during this fault event. It is worth noting that the cutoff frequency of the power loop LPFs affects the inverter passivity in both methods. For the proposed approach, a smaller ω_{LPF} results a smaller degree of passivity, but the system remains passive. In contrast, for the dVOC approach, a smaller ω_{LPF} leads to a deeper degree of the nonpassivity, making the system more likely to be unstable.

2) Transient Stability Analysis: The transient stability analysis of the proposed method and dVOC approach can also be conducted based on the dynamic equations of (25) and (26). By solving the equations with the MATLAB command "ode23," the phase portrait of $\dot{\delta} - \delta$ and $u - \delta$ can be obtained, and the system stability can then be predicted. Fig. 9 shows the phase portraits before, during, and after the short-to-ground fault with different cutoff frequencies of power loop LPFs. It can be observed that in the event of this short-circuit fault, the proposed control can maintain system stability after the fault is cleared, and the control voltage remains at 1, regardless of the cutoff frequency of LPFs. In contrast, the dVOC approach may lose synchronism and cannot return to stable operation after the fault is cleared, especially when the cutoff frequency of LPFs is small. The nonpassivity of the dVOC approach implies a sharp voltage drop when the fault occurs, which results in instability issues in certain cases.

3) Time-Domain Simulations Under Transient Events: Furthermore, to verify the passivity and transient stability analyses for the transient scenarios, time-domain simulations are also conducted in MATLAB/Simulink. The simulation results are depicted in Fig. 10. As demonstrated, the proposed control approach maintains system stability after the fault is cleared, and the system returns to its stable operating condition. However, the dVOC approach encounters transient stability issues due to the sharp voltage drop during the short-circuit fault if the cutoff frequency of the power loop LPFs is low. These results further support the passivity and transient stability analyses conducted earlier.

Based on the above analysis, it can be concluded that although the proposed control approach has a similar control structure as existing dVOC approaches, the passivity-based design achieved by the "*pumping-or-damping*" control action in the reactive power loop provides enhanced transient stability compared to the existing dVOC approach. This passivity-based design allows for stable connections of the GFMs to any passive grid without requiring system information for control parameter selection. Therefore, the proposed control approach has the potential to
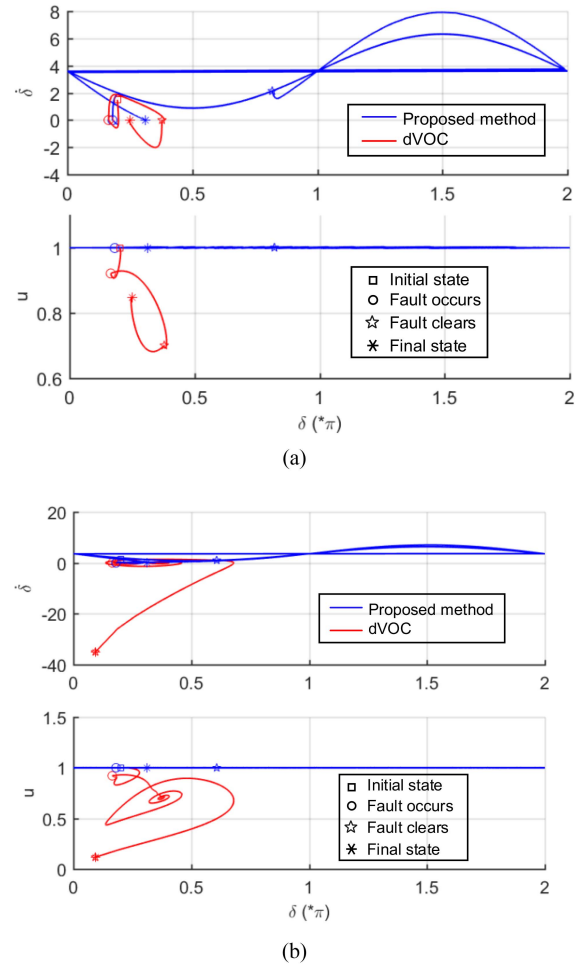

Fig. 9. Transient stability analysis of the proposed method and the dVOC approach with (a) $\omega_{\text{LPF}} = 20\pi$ rad/s and (b) $\omega_{\text{LPF}} = 2\pi$ rad/s.

be a more robust and reliable control method for grid-connected GFMs.

### C. Inverter Capability to Achieve Passivity

To achieve the passivity-based design, the requirements of the inverter capability are also investigated. Fig. 11 presents the simulation results of phase a current i_{La} and reactive power Q for both the dVOC approach and the proposed method during fault with $\omega_{\text{LPF}} = 2\pi$ rad/s. The simulation results reveal that the peak phase current during fault remains practically the same for both methods, at approximately 4 p.u. However, the proposed method exhibits a longer duration of overcurrent compared to the dVOC approach. Additionally, the reactive power during the fault is also higher for the proposed method compared to the dVOC approach.

These simulation waveforms in Figs. 10 and 11 convey two important messages. First, to achieve inverter passivity, it is necessary to maintain the control voltage, which, in turn, requires a higher inverter reactive capacity. Specifically, the proposed method can provide more reactive power to maintain control
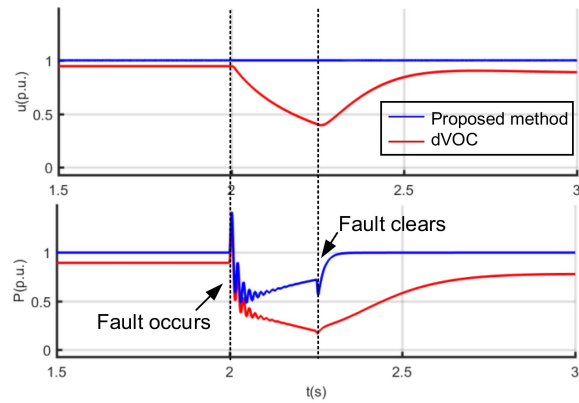
(a)
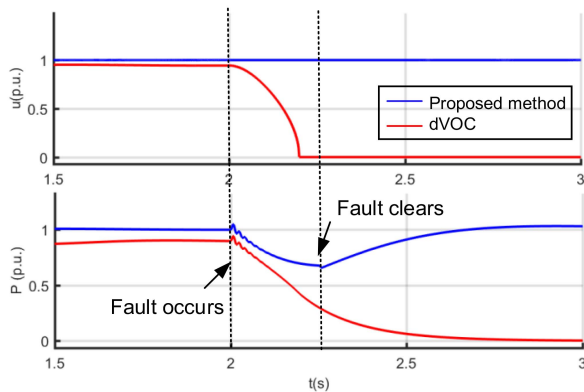
(b)

Fig. 10. Simulations of control voltage and active during the short-circuit-fault transient of the proposed method and the dVOC approach with (a) $\omega_{\text{LPF}} = 20\pi$ rad/s and (b) $\omega_{\text{LPF}} = 2\pi$ rad/s.
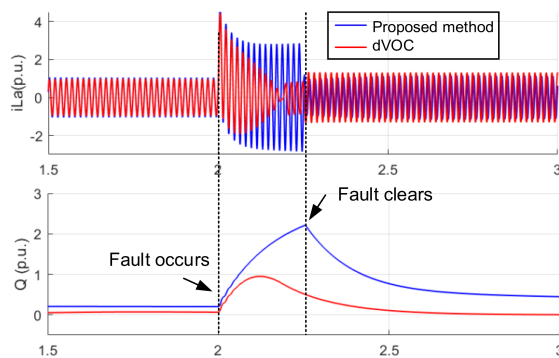

Fig. 11. Simulations of phase current and reactive power during the short-circuit-fault transient of the proposed method and the dVOC approach with $\omega_{\text{LPF}} = 2\pi$ rad/s.

voltage during the fault, ensuring system stability. In contrast, the dVOC approach experiences a sharp voltage drop during the fault, resulting in a loss of synchronism and an inability to return to a steady state after the fault is cleared. Second, the inverter rating is largely determined by the peak current due to the small thermal capacity of the inverter. Even though the proposed method requires a longer overcurrent duration than the dVOC approaches, they have similar peak currents, indicating
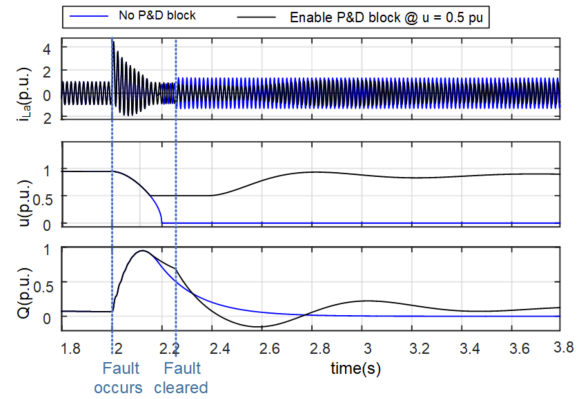

Fig. 12. Enabling "*pumping-or-damping*" block when u drops 0.5 p.u. in the proposed method.

that the proposed approach can achieve inverter passivity for better system stability with only a slight increase in inverter rating.

It is worth mentioning that the control voltage-regulation capability of the proposed method does not necessarily come from the reactive power capability that the hardware can withstand. Instead, the "*pumping-or-damping*" motion is the key factor in maintaining the voltage. This means that even if the reactive power capacity of the inverter is limited during transients, the "*pumping-or-damping*" motion facilitated by the proposed method can still help maintain the control voltage at a prespecified value and improve system stability. As demonstrated in Figs. 10 and 11, if the inverter can provide the necessary reactive power to match the system's transient requirements, the control voltage can be maintained at 1 p.u. However, in cases where the reactive power capability is constrained during a transient event, the presence of the "*pumping-or-damping*" motion in the proposed method can assist in maintaining the control voltage at the desired level. Fig. 12 illustrates this scenario: without the "*pumping-or-damping*" block, the system loses synchronism, whereas enabling the "*pumping-or-damping*" block when the control voltage drops to 0.5 p.u. allows for voltage clamping during the fault. As a result, the system can subsequently return to stable operation once the fault is cleared.

In summary, to ensure the passivity of the inverter, it is necessary to have extra reactive power capability or voltage amplitude regulation capability. This conclusion aligns with recent findings in the field [42].

V. CASE STUDY OF MULTI-INVERTER SYSTEMS WITH PROPOSED CONTROL APPROACH

A. Simulation Tests

To further demonstrate the feasibility and effectiveness of the proposed control approach in multi-inverter systems, simulations were conducted on a three-bus system, as shown in Fig. 13, to examine system transient stability under various operating conditions. Bus 1 is connected to an inverter that is controlled as an ideal voltage source and can be considered as a slack bus, which is connected to the system for all the simulated scenarios
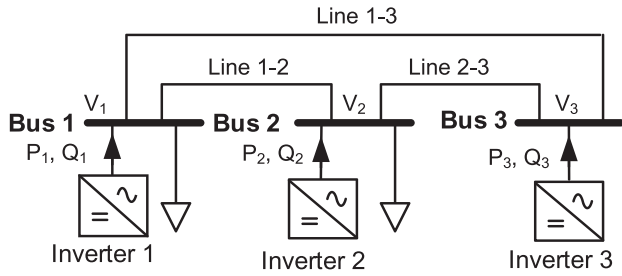
Fig. 13. Test of system with multiple inverters.

TABLE II
ELECTRICAL AND CONTROL PARAMETERS IN THE MULTI-INVERTER TEST SYSTEM

Variables		Value	Variables	Value
Bus voltage (V)		50	Lines 1 and 2 (p.u.)	0.18
Rated power (kVA)		1	Lines 1 and 3 (p.u.)	0.37
System frequency (Hz)		60	Lines 2 and 3 (p.u.)	0.11
Output inductance (mH)		2.4	Output capacitance (μF)	10
Control parameters	ξ_1	0.0605	$|\xi_2|$	0.42
	ξ_3	6.28	ε	10^{-5}

below. Bus 2 and Bus 3 are connected to Inverter 2 and Inverter 3, respectively, which are implemented with the proposed control approaches. All loads in the system are constant impedance loads.

The electrical and control parameters used for the simulations of the three-bus systems are given in Table II. Four transient scenarios were simulated, including a normal load transient, a short-circuit fault, an open-circuit fault, and a bus voltage drop. It is worth noting that the control parameters for these inverters were designed without the need for system information, such as transmission line parameters.

1) Normal Load Transient: In the first scenario, Inverter 2 acts as a source, providing 1 p.u. of active power to the system, while Inverter 3 initially operates as a load consuming 0.1 p.u. power; then the reference load power is increased to 1 p.u. at $t = 3$ s; and finally, it switches to generation mode with 1 p.u. output power at $t = 6$ s.

The simulation results in Fig. 14 show that the active power of Inverter 3 is regulated to the reference value in steady-state, and the active power of Inverter 2 is well regulated at predefined 1 p.u. The steady-state output voltages of Inverter 2 and Inverter 3 slightly drop to meet power requirements, while the frequencies all return to 60 Hz.

2) Short-Circuit Fault: In the second scenario, Inverter 2 and Inverter 3 both work as sources delivering 1 p.u. power to the rest of the system. A short-circuit fault with a 1 mΩ short resistor occurs at Bus 2 at $t = 2$ s and lasts for 100 ms.

As shown in Fig. 15, after the fault is cleared, the voltage, frequency, and power all return to the prespecified reference value. Also, the magnitudes of control voltages of all three inverters are given to prove that even during severe transient scenarios, the
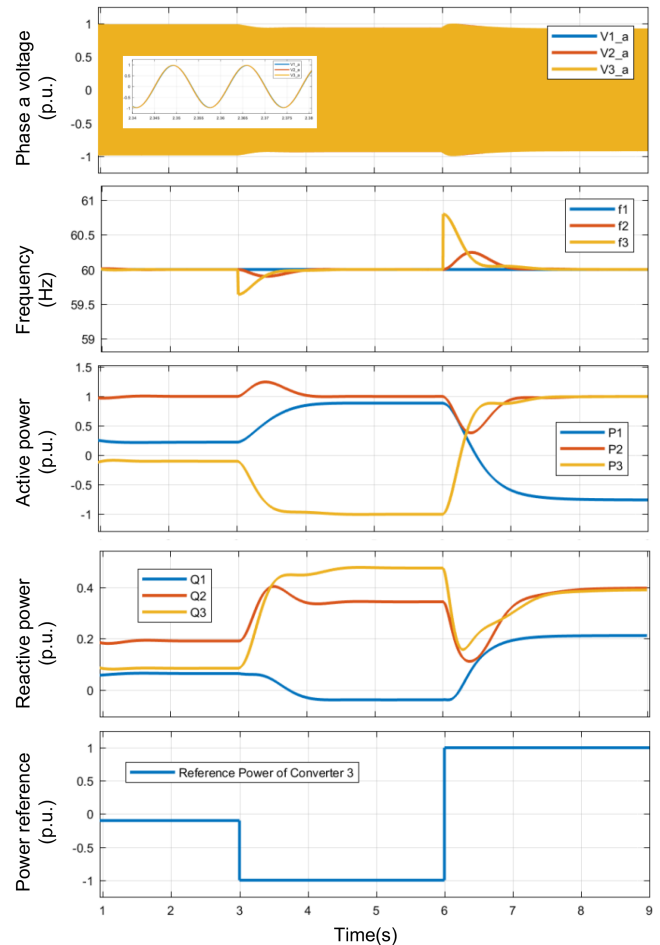

Fig. 14. System response under load transient.

control voltage can be maintained at 1 p.u., so that any potential transient stability issues caused by the sharp voltage drop [5] can be avoided. For the other less severe transient scenarios simulated in this article, the control voltage is not shown because it can be easily observed from the phase voltage waveforms that the magnitude almost stays unchanged. It is worth noting that in the above analysis, it is assumed that the fault conditions will not trigger the overcurrent protection of the inverter. The current limitation control scheme for VOC approaches is still an open issue and is beyond the scope of this research.

3) Open-Circuit Fault: In the third scenario, Inverter 2 and Inverter 3 continue to deliver 1 p.u. power to the system. At $t = 3$ s, Lines 2 and 3 experiences an open-circuit fault and remains disconnected from the system until it returns to service at $t = 6$ s. Two types of open-circuit faults can occur: one is that Lines 2 and 3 is totally out of service and disconnected from the system, and the other is that the impedance of Lines 2 and 3 changes from 0.1 to 0.2 p.u.

In the case of the first type of open-circuit fault, as shown in Fig. 16, the inverters are capable of regulating the output power and frequency during the fault and after the fault is cleared. Moreover, the output voltage will self-adjust according to the power flow.
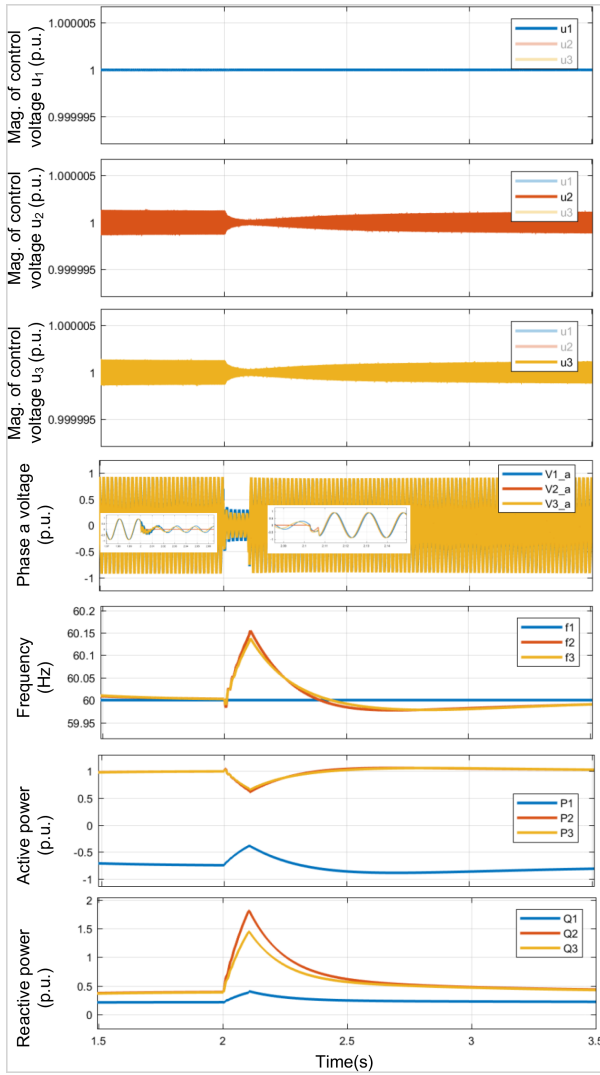
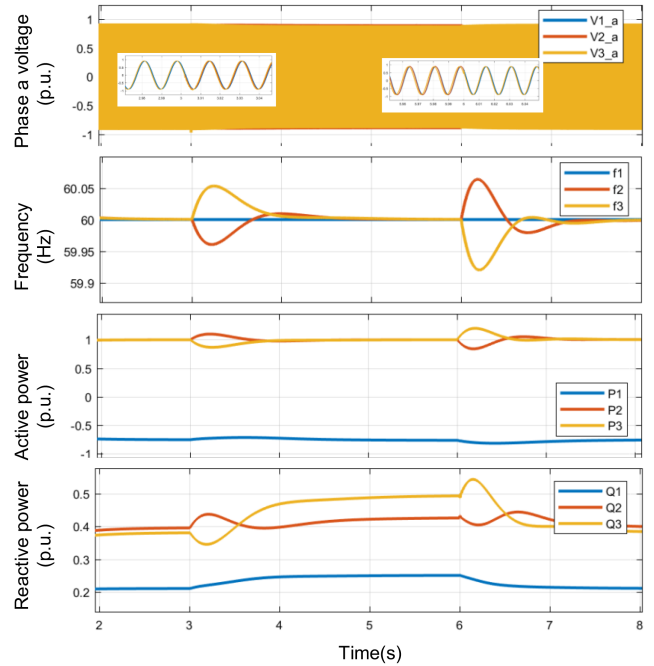Fig. 15.   System response during short-circuit fault.

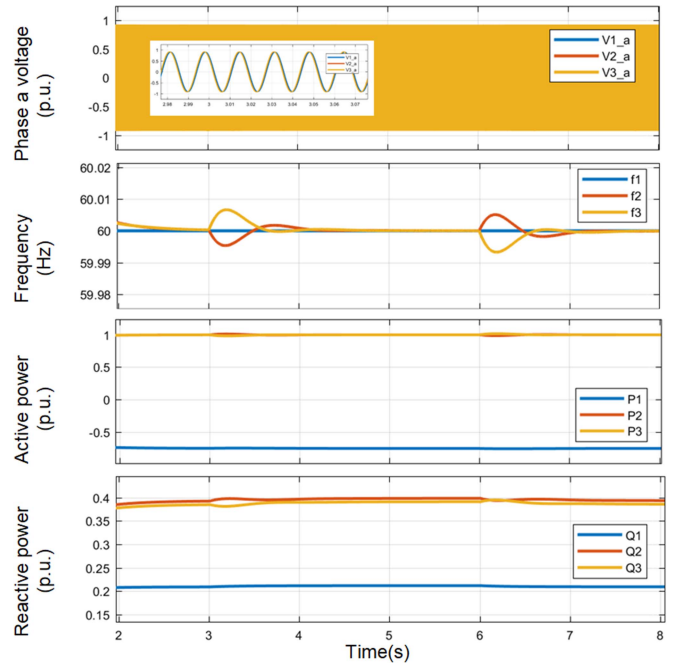Fig. 16.   System response during an open-circuit fault (Lines 2 and 3 disconnected).

Fig. 17.   System response during an open-circuit fault (impedance of Lines 2 and 3 change from 0.1 to 0.2 p.u.).

In the case of the second type of open-circuit fault, as shown in Fig. 17, the system remains stable during the fault and returns to the prefault operating conditions after the fault is cleared.

4) Bus Voltage Drop: In this scenario, Inverter 2 and Inverter 3 each deliver 1 p.u. power into the system. During the fault, it is assumed that the voltage on Bus 1 drops to 0.5 p.u. and the fault persists for 3 seconds.

As shown in Fig. 18, it is evident that Inverter 2 and Inverter 3 maintain synchronism with the grid and regulate the active power to 1 p.u. during the fault and after the fault is cleared. However, additional reactive power is required for Inverter 2 and Inverter 3 to regulate voltage during fault.

B. Experimental Tests

The above analysis and simulation results have already shown that the proposed control can ensure system stability under different grid conditions, owing to the *"pumping or damping"* motion in the reactive power loop. While the proposed controller has been extensively analyzed and simulated, it is challenging to replicate severe system disturbances in laboratory tests due to hardware constraints. Thus, to validate the efficacy of the proposed control approach and enable the design of stable multi-inverter systems, a six-inverter system, as depicted in Fig. 19, has been constructed in the hardware testbed (HTB) at CURENT UTK [43]. This experimental setup is subjected to a normal load
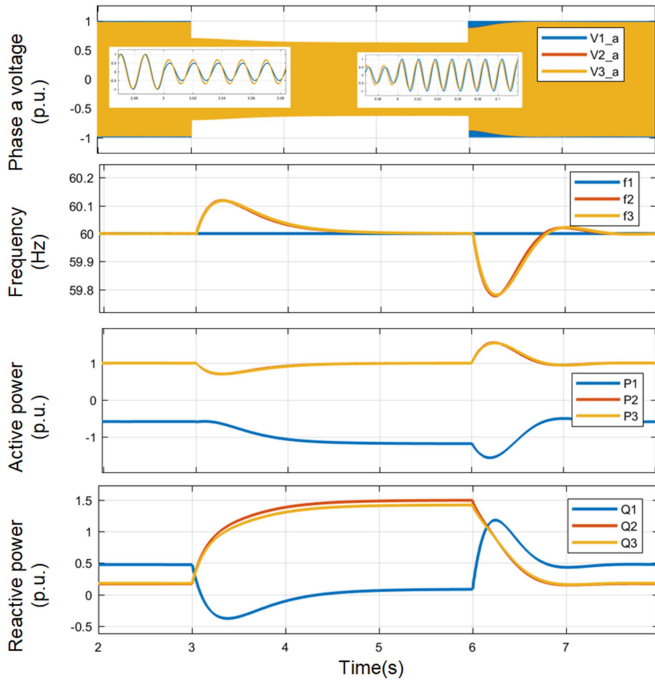
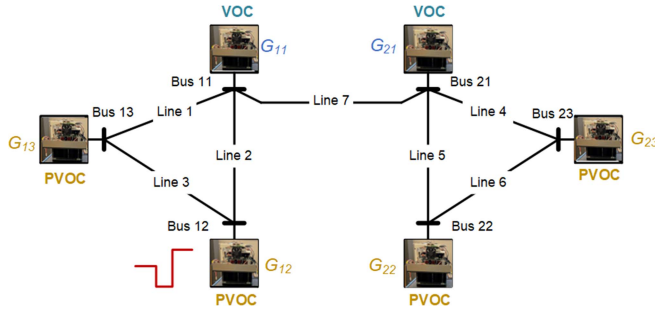Fig. 18.   System response during voltage drop at Bus 1.

Fig. 19.   Six-inverter test system.

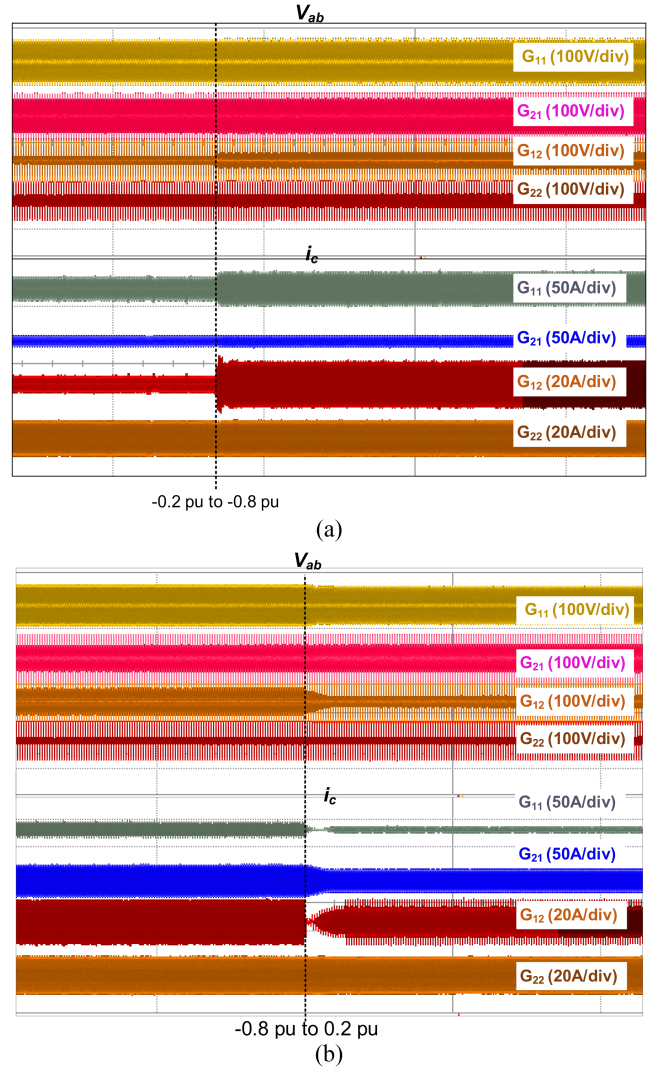-0.2 pu to -0.8 pu

(a)

-0.8 pu to 0.2 pu

(b)

Fig. 20.   Measured voltage and current waveforms of the six-inverter system. (a) Output power of G_{12} changes from 0.2 to 0.8 p.u. (b) G_{12} changes from generator mode with 0.8 p.u. power to load mode with 0.2 p.u. power.

step transient to confirm the proper functioning of the proposed controller.

In this six-inverter system, G_{11} and G_{21} are implemented with a simple virtual oscillator control that does not incorporate any power dispatching loop. All the other inverters are implemented with the proposed control approach with the control parameters in Table II. It is noteworthy that these control parameter designs do not employ any network information. The underlying assumption is that the system can reach an equilibrium point under its designated working conditions. For the HTB-based test, the inverter G_{12} operates as a generator initially, and delivers 0.2 p.u power to the system; then its output power is increased to 0.8 p.u.; after which, it transitions to load mode and consumes 0.2 p.u. power.

Figs. 20 and 21 show the test results of the six-inverter system under the normal load transient. It can be seen that the inverters with the proposed control approach can operate effectively as expected and uphold system stability during the load transient scenario.

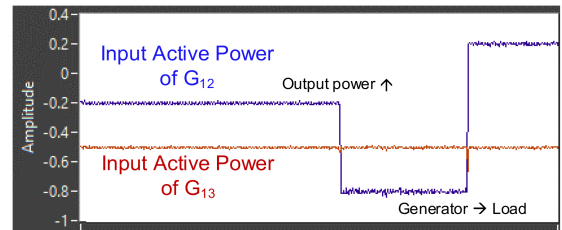Fig. 21.   Measured power in LabVIEW of G_{12} and G_{13} during power transient of G_{12}.

VI. CONCLUSION

This article proposes a passivity-based grid-forming control approach for grid-connected inverters, which is based on the CbI technique in the PH structure. Compared to the existing passivity-based virtual synchronous machine (VSM) control, the proposed approach has a simpler two-channel structure with

clear physical meaning. Specifically, the control comprises the active power-frequency (*p-f*) loop and the reactive power-voltage (*Q-u*) loop. Moreover, it shares similarities with the existing dVOC approach in terms of the heavily damped characteristics in the *p-f* loop. However, it enhances system transient stability under various grid conditions via the constant control voltage magnitude, achieved through the *"pumping-or-damping"* motion in the *Q-u* loop. The simulation and experimental results demonstrate that the proposed control approach can facilitate the transient stability design of a multi-inverter system by rendering each inverter in the system passive. Thus, the proposed control approach can enable effective grid-forming control, which is crucial for the integration of power electronic-based sources into power systems.

REFERENCES

[1] N. Hatziargyriou et al., "Definition and classification of power system stability—Revisited & extended," *IEEE Trans. Power Syst.*, vol. 36, no. 4, pp. 3271–3281, Jul. 2021.

[2] L. Kong, Y. Xue, L. Qiao, and F. Wang, "Review of small-signal converter-driven stability issues in power systems," *IEEE Open Access J. Power Energy*, vol. 9, pp. 29–41, 2022.

[3] Y. Lin et al., "Research roadmap on grid-forming inverters," U.S. Department of Energy, Office of Scientific and Technical Information, Oak Ridge, TN, USA, 2020. [Online]. Available: https://www.osti.gov/biblio/1721727

[4] R. H. Lasseter, Z. Chen, and D. Pattabiraman, "Grid-forming inverters: A critical asset for the power grid," *IEEE J. Emerg. Sel. Topics Power Electron.*, vol. 8, no. 2, pp. 925–935, Jun. 2020.

[5] H. Yu, M. A. Awal, H. Tu, I. Husain, and S. Lukic, "Comparative transient stability assessment of droop and dispatchable virtual oscillator controlled grid-connected inverters," *IEEE Trans. Power Electron.*, vol. 36, no. 2, pp. 2119–2130, Feb. 2021.

[6] D. Pan, X. Wang, F. Liu, and R. Shi, "Transient stability of voltage-source converters with grid-forming control: A design-oriented study," *IEEE J. Emerg. Sel. Topics Power Electron.*, vol. 8, no. 2, pp. 1019–1033, Jun. 2020.

[7] L. A. B. Tôrres, J. P. Hespanha, and J. Moehlis, "Power supply synchronization without communication," in *Proc. IEEE Power Energy Soc. Gen. Meeting*, 2012, pp. 1–6.

[8] Q.-C. Zhong, *Power Electronics-Enabled Autonomous Power Systems: Next Generation Smart Grids*. Hoboken, NJ, USA: Wiley, 2020.

[9] E. M. Navarro-López and E. Licéaga-Castro, "Combining passivity and classical frequency-domain methods: An insight into decentralised control," *Appl. Math. Comput.*, vol. 215, no. 12, pp. 4426–4438, 2010.

[10] H. Yu, M. A. Awal, H. Tu, Y. Du, S. Lukic, and I. Husain, "Passivity-oriented discrete-time voltage controller design for grid-forming inverters," in *Proc. IEEE Energy Convers. Congr. Expo.*, 2019, pp. 469–475.

[11] Y. Liao and X. Wang, "Passivity analysis and enhancement of voltage control for voltage-source converters," in *Proc. IEEE Energy Convers. Congr. Expo.*, 2019, pp. 5424–5429.

[12] G. Wu et al., "Passivity-based stability analysis and generic controller design for grid-forming inverter," *IEEE Trans. Power Electron.*, vol. 38, no. 5, pp. 5832–5843, May 2023.

[13] H. Wu and X. Wang, "Passivity-based dual-loop vector voltage and current control for grid-forming VSCs," *IEEE Trans. Power Electron.*, vol. 36, no. 8, pp. 8647–8652, Aug. 2021.

[14] Y. Qi, H. Deng, J. Wang, and Y. Tang, "Passivity-based synchronization stability analysis for power-electronic-interfaced distributed generations," *IEEE Trans. Sustain. Energy*, vol. 12, no. 2, pp. 1141–1150, Apr. 2021.

[15] F. Zhao, X. Wang, and T. Zhu, "Low-frequency passivity-based analysis and damping of power-synchronization controlled grid-forming inverter," *IEEE J. Emerg. Sel. Topics Power Electron.*, vol. 11, no. 2, pp. 1542–1554, Apr. 2023.

[16] N. Khefifi, A. Houari, M. Machmoum, M. Ghanes, and M. Ait-Ahmed, "Control of grid forming inverter based on robust IDA-PBC for power quality enhancement," *Sustain. Energy, Grids Netw.*, vol. 20, 2019, Art. no. 100276.

[17] P. Yang, F. Liu, Z. Wang, and C. Shen, "Distributed stability conditions for power systems with heterogeneous nonlinear bus dynamics," *IEEE Trans. Power Syst.*, vol. 35, no. 3, pp. 2313–2324, May 2020.

[18] Q.-C. Zhong and M. Stefanello, "A port-Hamiltonian control framework to render a power electronic system passive," *IEEE Trans. Autom. Control*, vol. 67, no. 4, pp. 1960–1965, Apr. 2022.

[19] D. Jeltsema and J. M. A. Scherpen, "Multidomain modeling of nonlinear networks and systems," *IEEE Control Syst. Mag.*, vol. 29, no. 4, pp. 28–59, Aug. 2009.

[20] S. Arjan van der and J. Dimitri, *Port-Hamiltonian Systems Theory: An Introductory Overview*. Hanover, MD, USA: Now Foundations and Trends, 2014.

[21] A. van der Schaft and H. Schumacher, *An Introduction to Hybrid Dynamical Systems*. Berlin, Germany: Springer, 1999.

[22] R. Rosso, X. Wang, M. Liserre, X. Lu, and S. Engelken, "Grid-forming converters: Control approaches, grid-synchronization, and future trends—A review," *IEEE Open J. Ind. Appl.*, vol. 2, pp. 93–109, 2021.

[23] L. Zhang, L. Harnefors, and H.-P. Nee, "Power-synchronization control of grid-connected voltage-source converters," *IEEE Trans. Power Syst.*, vol. 25, no. 2, pp. 809–820, May 2010.

[24] H. Wu and X. Wang, "Design-oriented transient stability analysis of grid-connected converters with power synchronization control," *IEEE Trans. Ind. Electron.*, vol. 66, no. 8, pp. 6473–6482, Aug. 2019.

[25] J. M. Guerrero, L. G. de Vicuna, J. Matas, M. Castilla, and J. Miret, "A wireless controller to enhance dynamic performance of parallel inverters in distributed generation systems," *IEEE Trans. Power Electron.*, vol. 19, no. 5, pp. 1205–1213, Sep. 2004.

[26] L. Yunwei, D. M. Vilathgamuwa, and L. Poh Chiang, "Design, analysis, and real-time testing of a controller for multibus microgrid system," *IEEE Trans. Power Electron.*, vol. 19, no. 5, pp. 1195–1204, Sep. 2004.

[27] W. Du et al., "A comparative study of two widely used grid-forming droop controls on microgrid small-signal stability," *IEEE J. Emerg. Sel. Topics Power Electron.*, vol. 8, no. 2, pp. 963–975, Jun. 2020.

[28] N. Pogaku, M. Prodanovic, and T. C. Green, "Modeling, analysis and testing of autonomous operation of an inverter-based microgrid," *IEEE Trans. Power Electron.*, vol. 22, no. 2, pp. 613–625, Mar. 2007.

[29] P. Hart and B. Lesieutre, "Energy function for a grid-tied, droop-controlled inverter," in *Proc. North Amer. Power Symp.*, 2014, pp. 1–6.

[30] B. B. Johnson, M. Sinha, N. G. Ainsworth, F. Dörfler, and S. V. Dhople, "Synthesizing virtual oscillators to control islanded inverters," *IEEE Trans. Power Electron.*, vol. 31, no. 8, pp. 6002–6015, Aug. 2016.

[31] B. B. Johnson, S. V. Dhople, A. O. Hamadeh, and P. T. Krein, "Synchronization of nonlinear oscillators in an LTI electrical power network," *IEEE Trans. Circuits Syst. I, Reg. Papers*, vol. 61, no. 3, pp. 834–844, Mar. 2014.

[32] G.-S. Seo, M. Colombino, I. Subotic, B. Johnson, D. Groß, and F. Dörfler, "Dispatchable virtual oscillator control for decentralized inverter-dominated power systems: Analysis and experiments," in *Proc. IEEE Appl. Power Electron. Conf. Expo.*, 2019, pp. 561–566.

[33] M. Lu, S. Dutta, V. Purba, S. Dhople, and B. Johnson, "A grid-compatible virtual oscillator controller: Analysis and design," in *Proc. IEEE Energy Convers. Congr. Expo.*, 2019, pp. 2643–2649.

[34] M. Colombino, D. Groß, J.-S. Brouillon, and F. Dörfler, "Global phase and magnitude synchronization of coupled oscillators with application to the control of grid-forming power inverters," *IEEE Trans. Autom. Control*, vol. 64, no. 11, pp. 4496–4511, Nov. 2019.

[35] L. Kong, Y. Xue, L. Qiao, and F. Wang, "Enhanced synchronization stability of grid-forming inverters with passivity-based virtual oscillator control," *IEEE Trans. Power Electron.*, vol. 37, no. 12, pp. 14141–14156, Dec. 2022.

[36] M. Sinha, F. Dörfler, B. B. Johnson, and S. V. Dhople, "Uncovering droop control laws embedded within the nonlinear dynamics of Van der Pol oscillators," *IEEE Trans. Control Netw. Syst.*, vol. 4, no. 2, pp. 347–358, Jun. 2017.

[37] M. Sinha, F. Dörfler, B. B. Johnson, and S. V. Dhople, "Virtual oscillator control subsumes droop control," in *Proc. Amer. Control Conf.*, 2015, pp. 2353–2358.

[38] M. Lu, V. Purba, S. Dhople, and B. Johnson, "Comparison of droop control and virtual oscillator control realized by Andronov-Hopf dynamics," in *Proc. 46th Annu. Conf. IEEE Ind. Electron. Soc.*, 2020, pp. 4051–4056.

[39] S. D. Arco and J. A. Suul, "Equivalence of virtual synchronous machines and frequency-droops for converter-based microgrids," *IEEE Trans. Smart Grid*, vol. 5, no. 1, pp. 394–395, Jan. 2014.

[40] X. Xiong, C. Wu, D. Pan, and F. Blaabjerg, "An improved synchronization stability method of virtual synchronous generators based on frequency feedforward on reactive power control loop," *IEEE Trans. Power Electron.*, vol. 36, no. 8, pp. 9136–9148, Aug. 2021.

[41] R. Ortega, A. van der Schaft, F. Castanos, and A. Astolfi, "Control by interconnection and standard passivity-based control of port-Hamiltonian systems," *IEEE Trans. Autom. Control*, vol. 53, no. 11, pp. 2527–2542, Dec. 2008.

[42] W. Si and J. Fang, "Transient stability improvement of grid-forming converters through voltage amplitude regulation and reactive power injection," *IEEE Trans. Power Electron.*, vol. 38, no. 10, pp. 12116–12125, Oct. 2023.

[43] L. M. Tolbert et al., "Reconfigurable real-time power grid emulator for systems with high penetration of renewables," *IEEE Open Access J. Power Energy*, vol. 7, pp. 489–500, 2020.

Liang Qiao (Graduate Student Member, IEEE) received the B.S. and M.S. degrees in electrical engineering from Xi'an Jiaotong University, Xi'an, China, in 2015 and 2018, respectively. He is currently working toward the Ph.D. degree in electrical engineering with the Department of Electrical Engineering and Computer Science, University of Tennessee, Knoxville, TN, USA.

His research interests include wide-bandgap devices, advanced gate drivers and stability analysis, and black-box modeling of power electronic-based power systems.

Le Kong (Member, IEEE) received the B.S. degree from the Nanjing University of Aeronautics and Astronautics, Nanjing, China, in 2014, the M.S. degree from the National Taiwan University, Taipei, Taiwan, in 2016, and the Ph.D. degree from the University of Tennessee, Knoxville, TN, USA, in 2022, all in electrical engineering.

From 2016 to 2017, she was an Application Engineer with the High-Power IC Department, Silergy Corporation, Hangzhou, China, focusing on system analysis and design of dc converters for power units. Since 2022, she has been an Application Engineer with Monolithic Power Systems, San Jose, CA, USA. Her research interests include power IC, power converters, and power-electronics-based power grids.
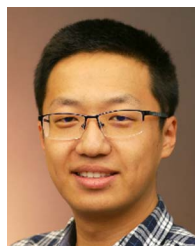
Yaosuo Xue (Senior Member, IEEE) received the B.Sc. degree in electrical engineering from East China Jiaotong University, Nanchang, China, in 1991, and the M.Sc. degree in electrical engineering from the University of New Brunswick, Fredericton, NB, Canada, in 2004.

From 1991 to 2000, he was an Electrical Engineer-in-Charge with the Ministry of Railways: Third Survey and Design Institute and led the traction power systems R&D for the first high-speed electric railway in China. During 2005 and 2006, he was a Lead Power Electronics and Systems Engineer with Capstone Turbine Corporation. During 2009–2015, he was a Research Manager and Scientist with Siemens Corporate Research and led Siemens Corporate Technology North America power electronics and energy management program and research. He is currently a senior R&D staff member and a Group Leader with Oak Ridge National Laboratory, Oak Ridge, TN, USA. His research interests include modeling, analysis, and control of all power electronic grids.

Mr. Xue is currently an Associate Editor for the IEEE TRANSACTIONS ON POWER ELECTRONICS and IEEE OPEN ACCESS JOURNAL OF POWER AND ENERGY. He is on the steering committee of the IEEE TRANSACTIONS ON TRANSPORTATION ELECTRIFICATION and assumes several leadership roles in IEEE Power Electronics Society TC1 and TC5, IEEE ITRD initiative, and IEEE ECCE.

Fei (Fred) Wang (Fellow, IEEE) received the B.S. degree from Xi'an Jiaotong University, Xi'an, China, and the M.S. and Ph.D. degrees from the University of Southern California, Los Angeles, CA, USA, in 1982, 1985, and 1990, respectively, all in electrical engineering.

From 1990 to 1992, he was a Research Scientist with the Electric Power Lab, University of Southern California. In 1992, he was an Application Engineer with the GE Power Systems Engineering Department, Schenectady, NY, USA. From 1994 to 2000, he was a Senior Product Development Engineer with GE Industrial Systems, Salem, VA, USA. From 2000 to 2001, he was the Manager of the Electronic & Photonic Systems Technology Lab, GE Global Research Center, Schenectady, NY, USA, and Shanghai, China. In 2001, he was a Research Associate Professor with the Center for Power Electronics Systems (CPES), Virginia Tech, Blacksburg, VA, USA, and became an Associate Professor in 2004. From 2003 to 2009, he was the CPES Technical Director. Since 2009, he has been with The University of Tennessee and Oak Ridge National Lab, Knoxville, TN, USA, as a Professor and the Condra Chair of Excellence in Power Electronics. He is a founding member and the Technical Director of the multiuniversity NSF/DOE Engineering Research Center for Ultra-wide-area Resilient Electric Energy Transmission Networks (CURENT) led by The University of Tennessee. His research interests include power electronics and power systems.

Dr. Wang is a Fellow of the U.S. National Academy of Inventors.